Electromagnetic Field in the Upper Ionosphere From ELF Ground-Based Transmitter

V. Pilipenko, Michel Parrot, E. Fedorov, N. Mazur

Correspondence to:
V. A. Pilipenko,
space.soliton@gmail.com

Electromagnetic Field in the Upper Ionosphere From ELF Ground-Based Transmitter

V. A. Pilipenko[1,2] ID **, M. Parrot[3]** ID **, E. N. Fedorov[1], and N. G. Mazur[1]**

[1]Institute of Physics of the Earth, Moscow, Russia, [2]Space Research Institute, Moscow, Russia, [3]LPC2E/CNRS, University of Orléans, LPC2E/CNRS, Orléans, France

Abstract The feasibility of detection of electromagnetic response in the upper ionosphere to ground large-scale extremely low frequency (ELF) transmitters (e.g., submarine communication systems) by low-orbiting satellites is discussed. Several times when the DEMETER satellite (660 km) was in the vicinity of the ELF transmitter on the Kola Peninsula, the electric and magnetic sensors operating in a burst mode detected a narrowband 82-Hz emission. The same emission associated with the ELF transmitter was observed by a ground-based magnetometer. We modeled the rate of the ELF wave energy leakage into the upper ionosphere from an oscillating 82-Hz linear current with an infinite length suspended above a high-resistive ground. A realistic altitudinal profile of the plasma parameters has been reconstructed with the use of the IRI ionospheric model. The modeled amplitudes and polarization of electromagnetic response of the upper ionosphere are in reasonable agreement with the properties of emission recorded by the satellite.

1. Introduction: Manmade Large-Scale ELF Transmitters

The response of the ionosphere to natural (e.g., thunderstorms; Inan et al., 2010) and man-made (e.g., radio transmitters; Rothkaehl & Parrot, 2005; Starks et al., 2008) electromagnetic disturbances in the atmosphere and on the ground has been thoroughly studied in the very low frequency range (> 1 kHz). Much less attention has been paid to the ultralow frequency (ULF) range (below fundamental Schumann resonance ~8 Hz) and the extremely low frequency (ELF) range (above the Schumann resonance, but ≪ 1 kHz). Indeed, any noticeable ULF-ELF emission efficiency may be expected only for extremely large emitting systems. Nonetheless, such man-made large-scale ELF transmitters do exist: these are aerials for communication with submarines. Such powerful ELF communication facilities (suspended aerials with a length about several tens of kilometers) have been constructed in the United States (installations "Seafarer" and "Sanguine" operated at 76 Hz); Wait, 1972, India at 3–30 Hz, and China (Wireless Electromagnetic Method system) at 0.1–300 Hz. A virtual ELF transmitter was attempted to be produced in the ionosphere by modulated radio heating (Lehtinen & Inan, 2008). Here we consider the ELF transmitter ZEVS operating at 82 Hz on the Kola peninsula southeast of Murmansk.

Electromagnetic field propagation along the conductive Earth surface from ELF emitting dipoles in the Earth-ionosphere waveguide has been well measured and modeled (Tereshenko & Tereshenko, 2017; Wait, 1977). Theoretical notions were supported by dedicated experiments (Fraser-Smith & Bannister, 1998; Nickolaenko, 2008; Sidorenko et al., 2014; Yano et al., 2010; Zhamaletdinov et al., 2015). Signals from the ZEVS transmitter were detected as far as at distances up to 10,000 km (Interaction, 2014).

At the same time, a possibility of the ELF wave energy leakage into the upper ionosphere and feasibility of its detection by low-Earth orbit (LEO) satellites have not been adequately examined. The first and only report on detection of the ZEVS emission by the DEMETER satellite when it was close to the emission area was mentioned in the review by Parrot (2018).

In this paper we investigate theoretically the efficiency of the ELF wave excitation in the upper ionosphere by a linear near-Earth current using an elaborated numerical model with a realistic ionospheric profile. The vertical and horizontal structures of the wave amplitude in the atmosphere-ionosphere have been numerically modeled. For the theoretical model validation, the modeling results are compared with ELF emission observations in a burst mode in several events when the DEMETER satellite was in the vicinity of the ZEVS transmitter.
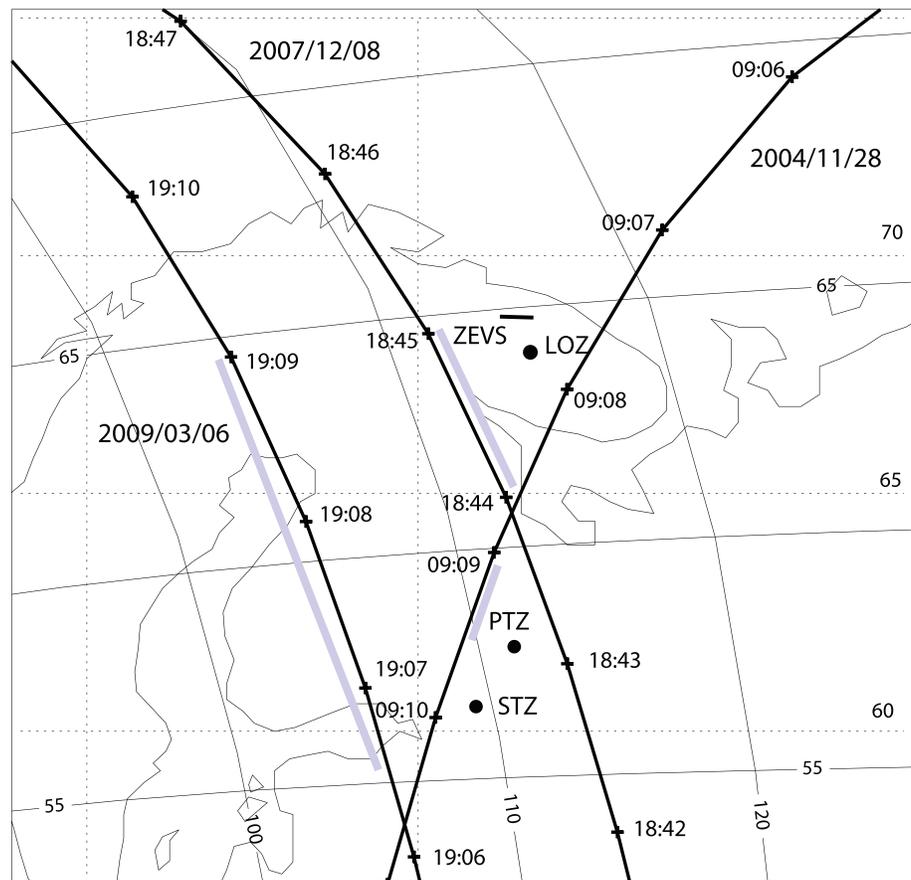
Figure 1. The vertical projection of the DEMETER orbit for the events 6 March 2009, 8 December 2007, and 28 November 2004. The locations of ZEVS and ground magnetometers are marked. Solid isolines denote the geomagnetic coordinates, and dotted isolines denote the geographic coordinates. Gray lines near the orbits indicate the intervals of the narrowband 82-Hz emission occurrence in satellite instruments.

2. Detection of Electromagnetic Response to Ground ELF Transmitter by DEMETER

Oppositely to very low frequency transmitters that have aerial antennae, emission in the ELF range needs specific devices to be efficient. To communicate with submarines below water and ice, the Russian Navy deployed the ELF transmitter ZEVS on the Kola peninsula. ZEVS consists of two parallel horizontal grounded antennas about 60 km in length that emit at 82 Hz. Emitted signal is frequency-modulated with frequency variations in the band of 81.0–83.3 Hz. Transmitter lines are elongated nearly in the east-west direction at the latitude of about 68°48′ N (Figure 1). The local noon/midnight at the ZEVS meridian is about 09/21 UT. The transmitter pumps a current up to 200–300 A and power up to 2.5 MW.

DEMETER was an ionospheric LEO microsatellite in operation between June 2004 and December 2010. Its orbit was circular (altitude 660 km), polar, and nearly Sun-synchronous (10.30 and 22.30 LT). Its payload measured electromagnetic waves in different frequency ranges from ULF to MF. One electric and one magnetic spectrogram up to 20 kHz were always onboard calculated with a low time (2 s) and frequency (19 Hz) resolution. But from time to time, the wave experiment was in the burst mode which allowed to record waveforms of six electromagnetic field components with sampling frequency 2.5 kHz. The data may be presented either in a satellite coordinate system $\{X_s, Y_s, Z_s\}$ or in a field-aligned coordinate system $\{X_b, Y_b, Z_b\}$ linked to local geomagnetic field: Z_b is along $\mathbf{B}_0$. Details of the wave experiment can be found in Berthelier et al. (2006) and Parrot et al. (2006).
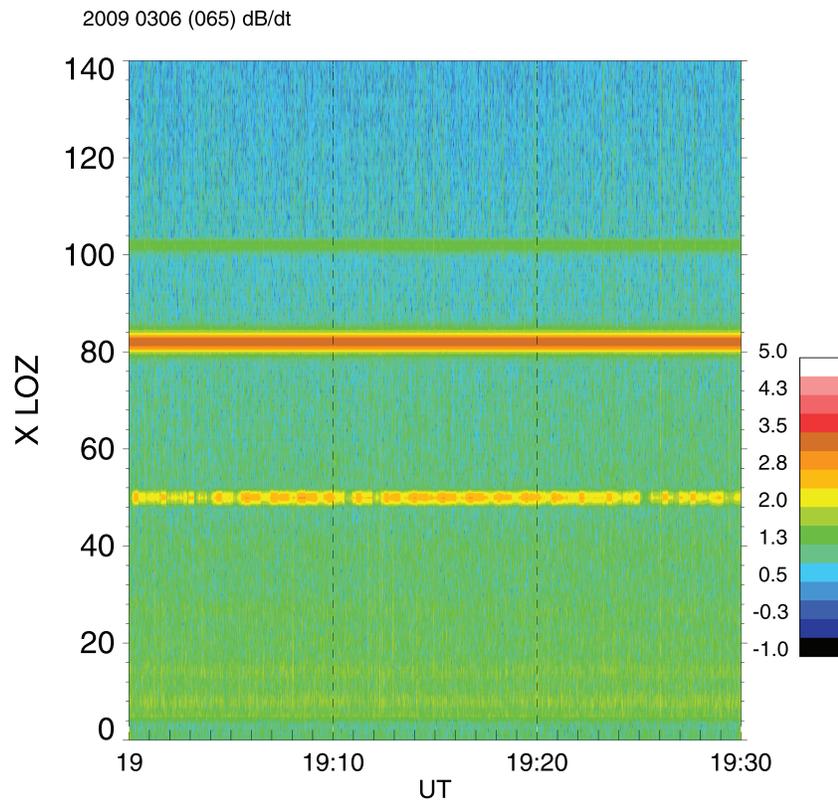
2009 0306 (065) dB/dt

Figure 2. Dynamic spectra (sonogram) from search coil magnetometer (*X*-component) at Lovozero (LOZ) during 6 March 2009 event (0900-0930 UT).

To be able to reveal the ZEVS-associated emissions, the satellite acquisition systems must be in the burst mode. Additionally, the satellite orbit must be close enough to ZEVS, and the transmitter must be on. Therefore, just a few rare events have been found so far.

2.1. The Nighttime Event on 6 March 2009

The data for this day from the search coil magnetometer at the ground station Lovozero (separated by $R = 89$ km from the transmitter) are available (Figure 1). The sonogram of the ground magnetometer for this day shows an occurrence of harmonics of power transmission lines at frequencies 50, 100, and 150 Hz and Schumann resonances (Figure 2). Also, signals from the ZEVS system are visible at 82 Hz.

On this day the closest approach of the DEMETER orbit passed near the ZEVS location during nighttime (Figure 1). The vertical projection of the orbit passed at a horizontal distance $R \simeq 533$ km from the ZEVS location (taken to be at $68°45'$ N, $34°20'$ E). During the time interval of 1906:30-1909:00 UT, the satellite detected a narrowband emission at a frequency of approximately 82 Hz. Sonograms of electric E_y and magnetic B_x components in the satellite reference system are shown in Figure 3. This emission was most evident in the electric component; the signal is less evident in the magnetic component. Lack of one-to-one correspondence between the occurrence of E and B emissions is caused by different background noise levels for electric and magnetic noise.

Spectral powers W_B and W_E of electric E_y and magnetic B_x components are given in Figure 4. The spectra were estimated with the periodogram method by averaging several individual fast Fourier transform spectra in a time window of 2,048 points. The spectral power of the component E_z is below the noise level and not shown.

The spectral power densities may be converted into a signal's amplitude as follows: $B(\text{nT}) \simeq \sqrt{W_B(\text{nT}^2/\text{Hz}) \times \Delta f(\text{Hz})}$ and $E(\mu\text{V/m}) \simeq \sqrt{W_E(\mu\text{V/m/Hz}) \times \Delta f(\text{Hz})}$, where the bandwidth of the recorded signal is Δf. For the spectral parameters in Figure 4, $\Delta f \simeq 3$ Hz, and the estimate of the signal amplitude gives $B_y \simeq 1.4$ pT, $E_y \simeq 15.4$ μV/m.
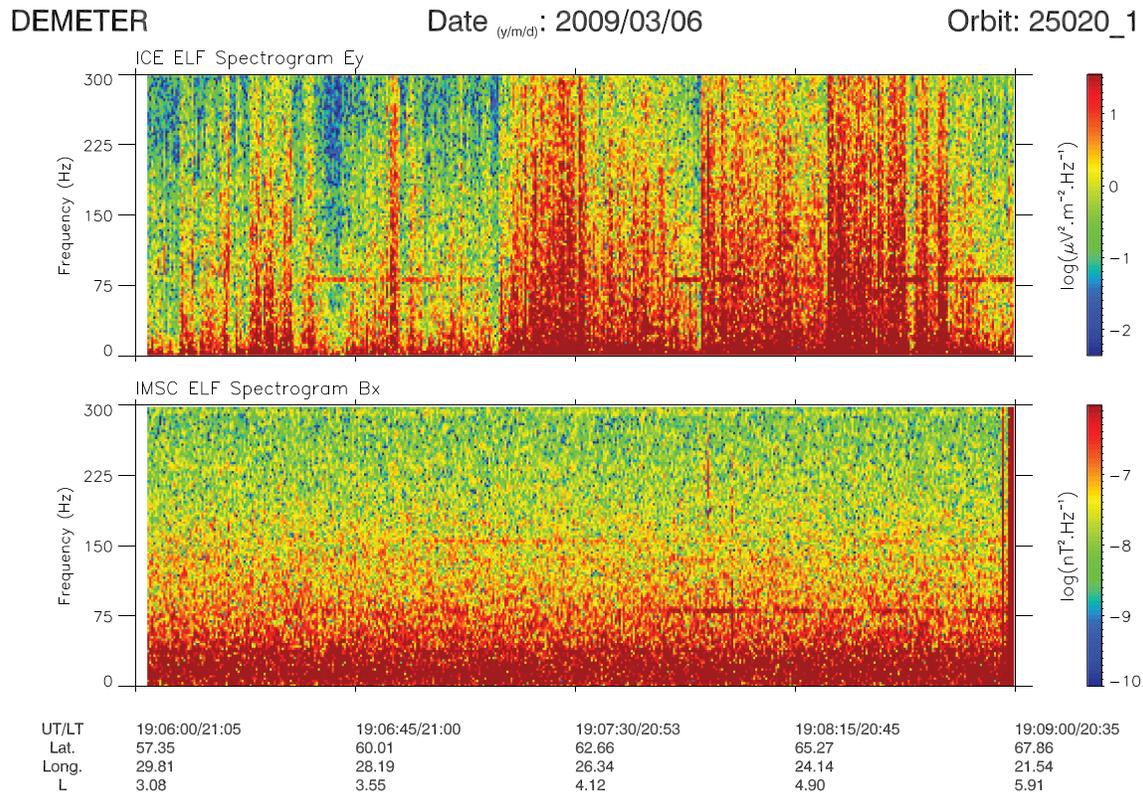
Figure 3. Sonogram of the event on 6 March 2009, 1906–1909 UT, for E_x and B_y components recorded by DEMETER. The frequency range is up to 300 Hz. The intensity is color coded according to the scales on the right. In the bottom, the geographic latitude and longitude are indicated, together with the L value.

2.2. The Nighttime Event on 8 December 2007

During this event the DEMETER orbit passed near the ZEVS location at nighttime (Figure 1). The closest approach of the vertical projection of the orbit passed at a horizontal distance $R \simeq 163$ km from the ZEVS location.

The sonogram of E_x and B_y components (in the satellite coordinate system) is shown in Figure 5. In the interval of 1844–1845 UT the electric and magnetic sensors detected the narrowband electromagnetic emission at the frequency of about 82 Hz. The signature of this emission is quite evident, although there was a lot of noise and turbulence in the electric spectrogram because the satellite was close to the auroral zone.

The static spectra of the power of the transverse magnetic and electric components are shown in Figure 6 in the field-aligned reference system. The amplitudes of the magnetic and electric components are estimated to be $B_y \simeq 4.5$ pT and $E_x \simeq 100$ µV/m.

A wave propagation analysis of the event on 8 December 2007 has been done with the PRASSADCO software which uses the six components of the electromagnetic field in a B_0-aligned frame of reference (Santolik et al., 2003). The analysis results are shown in Figure 7. The two top panels represent the spectrograms of the electric (a) and magnetic (b) fields where the emission at 82 Hz is clearly seen. Then the ellipticity ϵ_B is given in (c) using the singular-value decomposition method. At the ZEVS frequency, it shows an emission with a right-handed (RH) circular polarization. It is confirmed by the next panel (d) which gives the sense of polarization C_B with a higher level of confidence when the values are larger than +1 (Santolik et al., 2001). The two other panels are related to the direction of the wave vector **k** given by the method of Means (1972). It shows that the polar angle θ is small (e), so the direction of the **k** vector is aligned with B_0. This is confirmed by the last panel (g) which represents the direction of propagation of the parallel z-component of the Poynting vector P_z. Negative values of P_z correspond to the energy flux in the opposite direction of **B**$_0$. As the satellite is in the Northern Hemisphere it means that the recorded emission is upgoing.
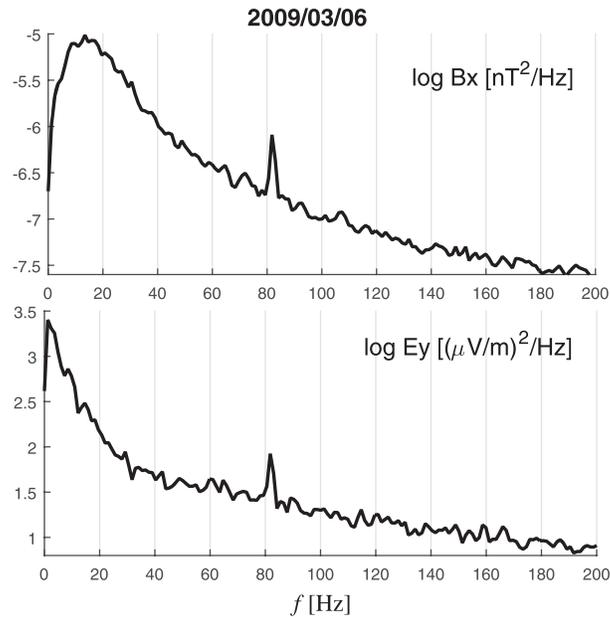
Figure 4. Fourier power spectra of E_x and B_y components for the event of 6 March 2009, recorded by DEMETER satellite during time interval 19.07.30–19.09.00 UT.

2.3. The Daytime Event on 28 November 2004

During time interval 0910–0911 UT DEMETER was near noon above ZEVS (Figure 1). The vertical projection of the orbit passed at a horizontal distance $R \simeq 177$ km from the ZEVS location at 0907:30 UT.

The satellite observed a weak narrowband emission at a frequency around 82 Hz (Figure 8). Signal in the satellite reference system can hardly be seen in the time interval 0910:00–0910:30 UT in E_x and B_y components.

Spectral power of electric and magnetic components is shown in Figure 9. During this daytime event the intensity of the 82-Hz emission is lower than in the two other nighttime events, as expected. The emission amplitudes estimated from the static power spectra are $B_y \simeq 1$ pT and $E_x \simeq 3.4$ μV/m.

3. Modeling the Electromagnetic Field of a Horizontal Line Current Above a Conducting Ground

As a theoretical foundation for the results of the satellite observations we have developed a numerical model. This multilayered horizontally homogeneous model with a realistic ionospheric vertical profile and a vertical geomagnetic field is similar to the model used for ULF observations in Fedorov et al. (2016) and Mazur et al. (2018).

3.1. Model and Basic Equations

We consider electromagnetic field only in the vicinity of the ELF transmitter (about several hundreds of kilometers and less). For such distances the account for a spherical Earth, as in Nickolaenko et al. (2016), is not necessary, and the Cartesian geometry is a very good approximation.

The tensor of relative dielectric permeability of the ionospheric plasma $\varepsilon' = \varepsilon/\varepsilon_0$ (where ε_0 is the vacuum dielectric permeability) in the field-aligned coordinate system has the form

$$\varepsilon' = \begin{pmatrix} \varepsilon_\perp & ig & 0 \\ -ig & \varepsilon_\perp & 0 \\ 0 & 0 & \varepsilon_\parallel \end{pmatrix}.$$

The standard formulas for the elements of the dielectric permeability tensor ε can be found elsewhere (e.g., Ginzburg, 1970).

The axis Z of the Cartesian coordinate system is chosen to be vertical upward with $z = 0$ on the ground, whereas X is southward, and Y is eastward. We assume that the electromagnetic field is excited by an
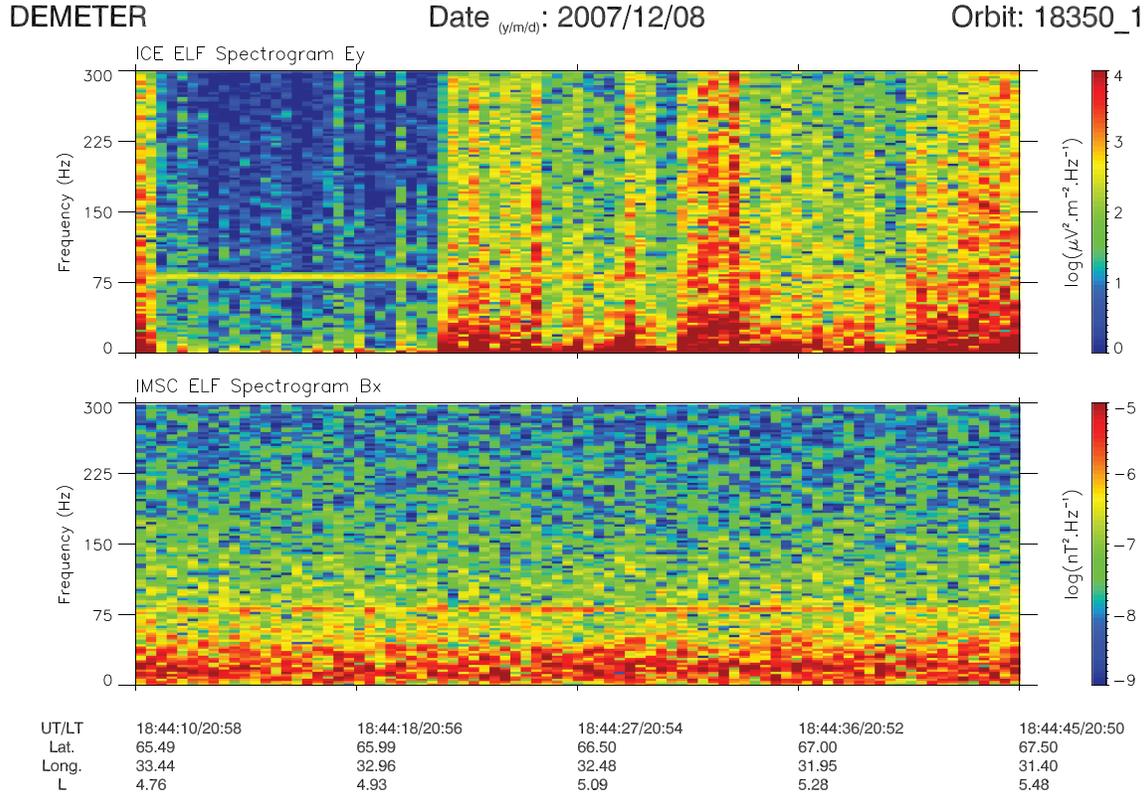
DEMETER   Date $_{(y/m/d)}$: 2007/12/08   Orbit: 18350_1

Figure 5. The same format of spectrogram as in Figure 3 but for the event of 8 December 2007, 1844–1845 UT for E_y and B_x components.

infinitely long line current along axis Y ($x = 0$), situated at altitude h above the Earth's surface and oscillating with frequency ω. A transmitter generates in the aerial, a periodic homogeneous along the y current $J(t) = J_0 \exp(-i\omega t)$. Therefore, the density of the driver current is $\mathbf{j}(x, z, t) = J_0 \exp(-i\omega t)\delta(x)\delta(z - h)\hat{\mathbf{y}}$.

We search the solutions of Maxwell's equations for magnetic $\mathbf{B}(x, z, t)$ and electric $\mathbf{e}(x, z, t) \equiv c^{-1}\mathbf{E}$ components as a time space harmonic $\propto \exp(-i\omega t)$. The spatial structure across the source current is given by a Fourier integral over the wavenumber k_x. In the transformed Maxwell's equations, the spatial spectral components $\mathbf{B}(k_x, z)$ and $\mathbf{e}(k_x, z)$ are related to the external driver current density $\mathbf{j}(k_x, z) = (2\pi)^{-1}J_0\delta(z-h)\hat{\mathbf{y}}$.

For simplicity the geomagnetic field is assumed to be vertical (i.e., the inclination of geomagnetic field $I = 90°$). Maxwell's equations for horizontal (tangential to the ionosphere) spatial spectral components $\mathbf{B}_\tau(k_x, z) = (B_x, B_y)$ and $\mathbf{e}_\tau(k_x, z) = (e_x, e_y)$ may be presented in the following matrix form

$$\partial_z\mathbf{B}_\tau - \mathbf{T}^{bb}\mathbf{B}_\tau = \mathbf{T}^{be}\mathbf{e}_\tau + \mu_0(2\pi)^{-1}J_0\delta(z - h)\hat{\mathbf{x}}$$
$$\partial_z\mathbf{e}_\tau - \mathbf{T}^{ee}\mathbf{e}_\tau = \mathbf{T}^{eb}\mathbf{B}_\tau$$

(1)

This system is similar to the one from (Fedorov et al., 2016). The system (1) of four linear first-order ordinary differential equations for horizontal field components $\mathbf{B}_\tau$ and $\mathbf{e}_\tau$ is obtained after the exclusion of the vertical components B_z and e_z from the complete Maxwell's system. For a vertical geomagnetic field the matrices $\mathbf{T}^{bb} = \mathbf{T}^{ee} = 0$, and the matrices $\mathbf{T}^{be}$ and $\mathbf{T}^{eb}$ are as follows:

$$T_{be} = \frac{i}{k_0}\begin{pmatrix} \pm ik_0^2 g & k_x^2 - k_0^2\varepsilon_\perp \\ k_0^2\varepsilon_\perp & \pm ik_0^2 g \end{pmatrix},$$

$$T_{eb} = ik_0\begin{pmatrix} 0 & 1 - k_x^2(k_0^2\varepsilon_\parallel)^{-1} \\ -1 & 0 \end{pmatrix}.$$

Here $k_0 = \omega/c$ is the wavenumber of a free space, the sign plus/minus symbol corresponds to the Southern/Northern Hemispheres.
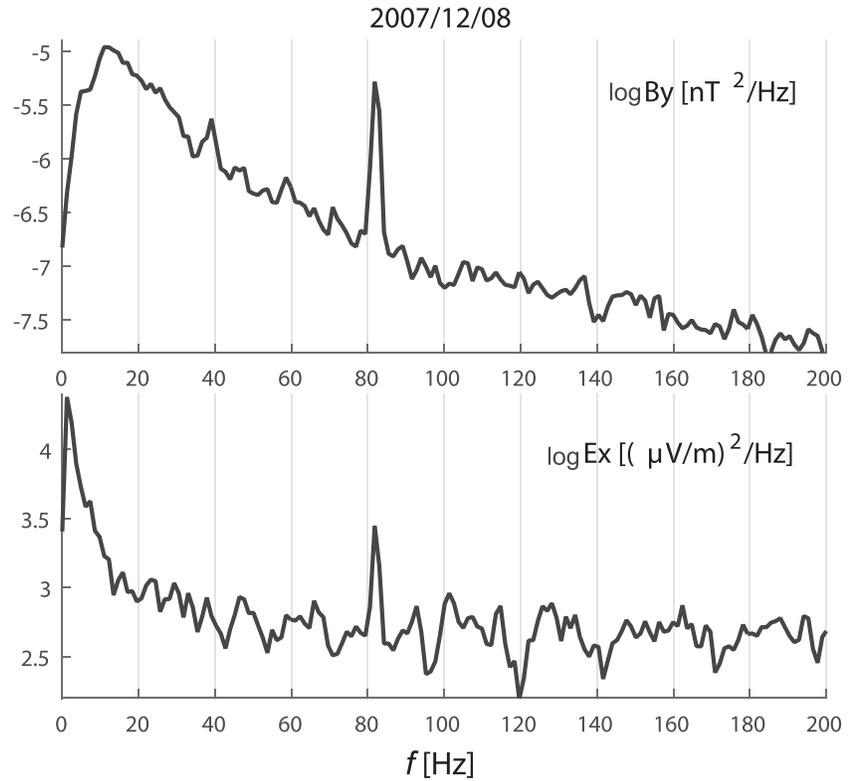
Figure 6. Power spectra of E_y and B_x components recorded by DEMETER for the event of 8 December 2007, 18.44.20–18.44.40 UT.

The outline of our mathematical approach to numerical solution of the problem is as follows. Further consideration is based on the use of the spectral admittance matrix $\mathbf{Y}$ relating the wave electric and magnetic components as follows: $\mathbf{B}_\tau = \mathbf{Y}\mathbf{e}_\tau$. The admittance matrix is normalized by the admittance of the free space $Y_0 = \sqrt{\varepsilon_0/\mu_0}$. This matrix will be shown to obey the generalized Riccati differential equation. The solution of Maxwell's equations under relevant boundary conditions will be reduced to the Cauchi problem with boundary conditions at the source (linear current) level. Solving the Cauchy problem upward from the source level and downward to the Earth provides a comprehensive definition of the vertical structure of the wave field.

3.2. Boundary Conditions

Maxwell's equations for the spatial spectra of the electromagnetic field will be solved numerically with allowance of the boundary emission condition in the topside ionosphere and impedance condition at the Earth's surface.

The horizontal electromagnetic components must match the boundary condition at the Earth's surface ($z = 0$) as follows: $\mathbf{B}_\tau = \mathbf{Y}_g\mathbf{e}_\tau$. We consider the Earth as a homogeneous half-space with the homogeneous conductivity σ_g. The normalized ground admittance matrix is

$$\mathbf{Y}_g = \begin{pmatrix} 0 & Y_g^{(H)} \\ -Y_g^{(E)} & 0 \end{pmatrix},$$

where the partial admittances for electric and magnetic modes are $Y_g^{(H)} = \kappa_g$ and $Y_g^{(E)} = \varepsilon_g/\kappa_g$, with the following notations used: $\varepsilon_g = \mathrm{Re}\,\varepsilon_g + i\sigma_g/(\omega\varepsilon_0)$ and $\kappa_g = \sqrt{\varepsilon_g - (k_x/k_0)^2}$.

Also, the emission condition at $z \to \infty$ must be fulfilled. The emission condition assumes that at $z \to \infty$ the excited electromagnetic field is a combination of outgoing waves $\propto \exp(+ik_zz)$. The field-aligned wave vector k_z found from the local dispersion equation for the vertical geomagnetic field, infinite scale along the
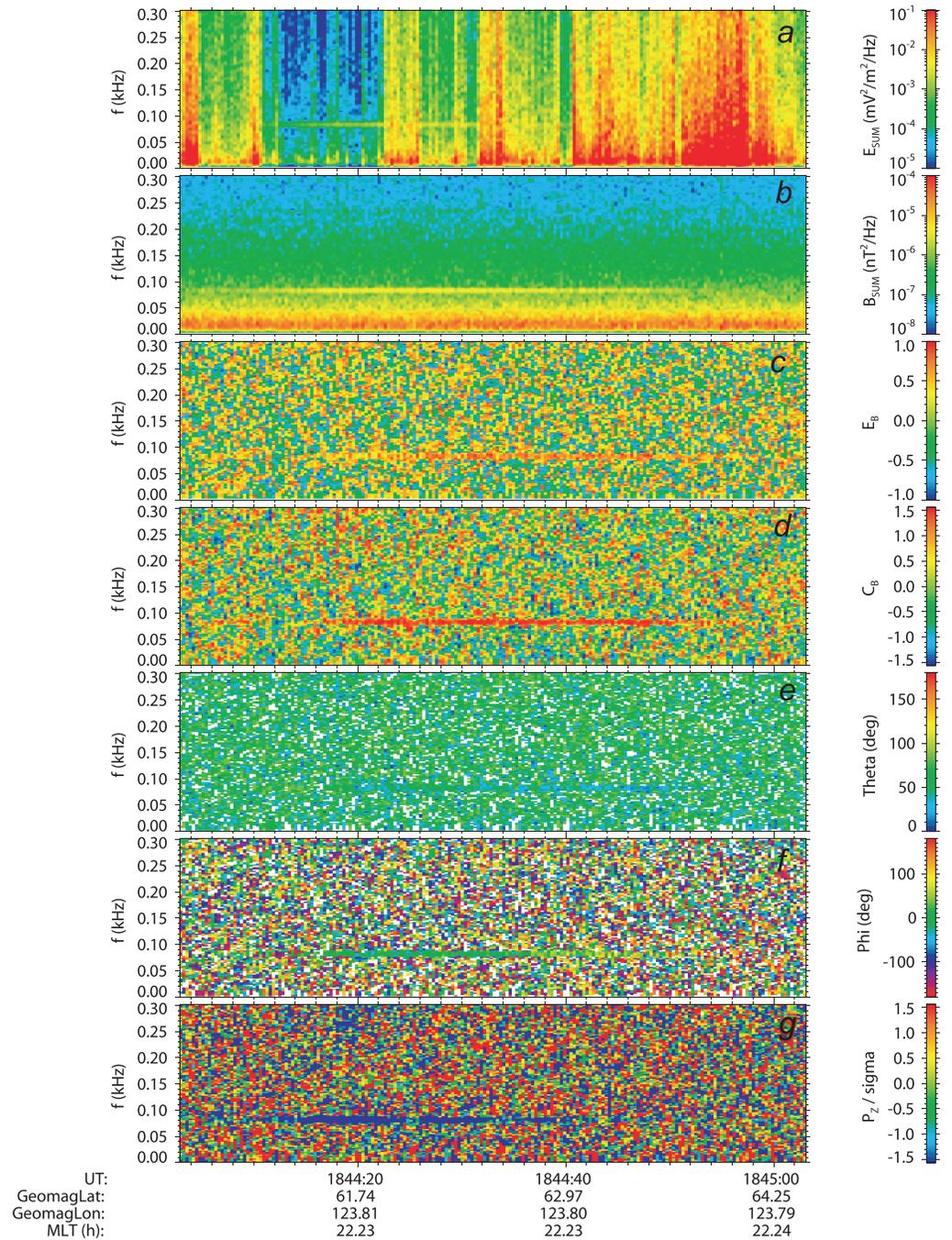
Figure 7. Wave propagation analysis of the event recorded on 8 December 2007 between 1844:02 and 1845:03 UT. From the top to the bottom, the panels display (a) the spectrogram from 0 up to 300 Hz of the electric field using the three components, (b) the spectrogram of the magnetic field using the three components, (c) the ellipticity ϵ_B, (d) the sense of polarization C_B, (e) the polar angle θ related to the direction of propagation of the **k** vector, (f) the azimuth angle ϕ related to the direction of the **k** vector, and (g) the direction of propagation of the parallel component of the Poynting vector P_z.

DEMETER   Date $_{(y/m/d)}$: 2004/11/28   Orbit: 02166_0
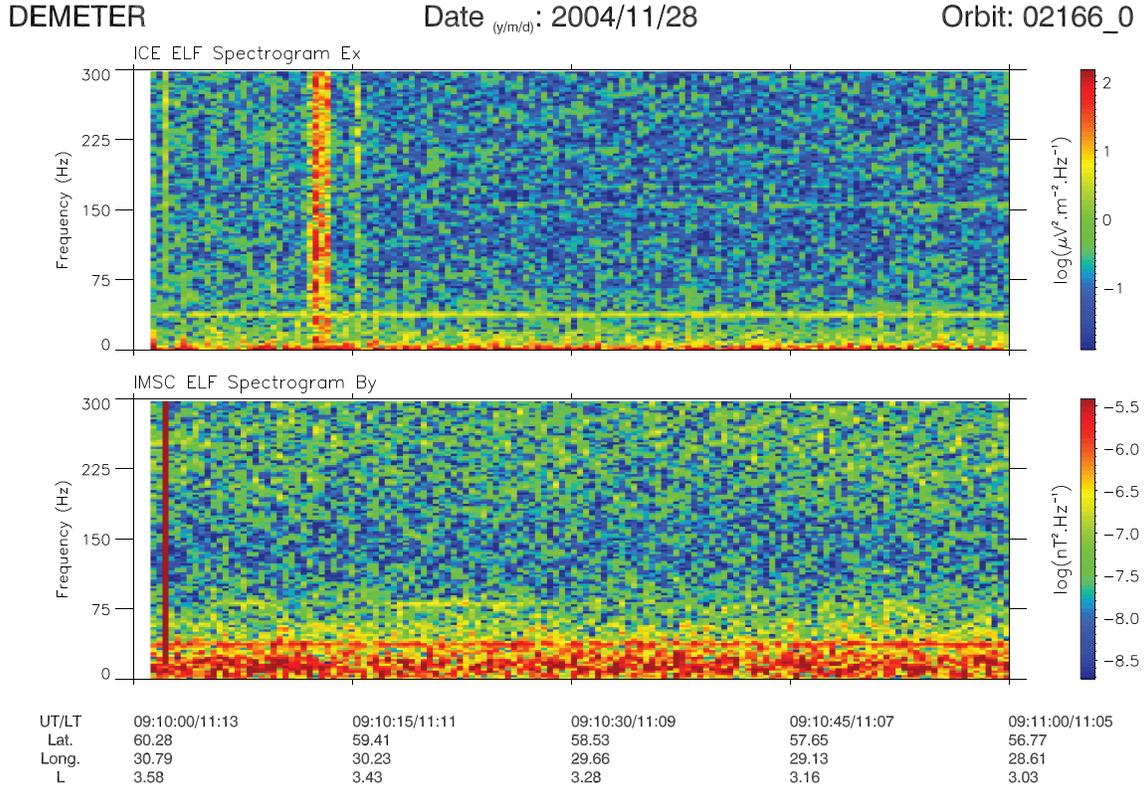

Figure 8. The same format of sonogram as in Figure 3 but for the event of 28 November 2004, 0910–0911 UT for E_x and B_y components.

source current $k_y = 0$ and fixed k_x is as follows:

$$k_z^2 = k_0^2 \varepsilon_\perp - \frac{1}{2}\left[k_x^2 \pm \sqrt{k_x^4 + 4k_0^4 g^2}\right]. \tag{2}$$

The sign plus/minus corresponds to RH/left-handed (LH) modes. Here the terms $\sim \varepsilon_\perp / \varepsilon_\parallel$ have been omitted.

The matching conditions at the source level $z = h$ must be fulfilled: the horizontal component of the electric field is to be continuous, whereas the magnetic component has a discontinuity as follows:

$$\mathbf{e}_\tau(h+0) - \mathbf{e}_\tau(h-0) = 0, \quad \mathbf{B}_\tau(h+0) - \mathbf{B}_\tau(h-0) = \mathbf{s} \equiv (2\pi)^{-1}\mu_0 J_0 \begin{pmatrix} 1 \\ 0 \end{pmatrix}. \tag{3}$$

The latter condition follows from integration of equation (1) through the source level plane, that is, from $h - 0$ to $h + 0$. The discontinuity of $\mathbf{B}_\tau$ is related to the driver current intensity J_0.

3.3. Calculation of Vertical Structure of Electromagnetic Field

The solution of Maxwell's equations under relevant boundary conditions has been reduced to the Cauchi problem with boundary conditions at the source (linear current) level. Then, by a numerical solution of the two boundary value Cauchy problems for equation (4), namely, from above to the source level and upward from the Earth's surface to the source level, the admittance matrix $\mathbf{Y}(z)$ will be found. A difference between its upper and lower limits at the source level, $\mathbf{Y}(h+0) \neq \mathbf{Y}(h-0)$, enables us to determine boundary values of magnetic and electric horizontal components at the source level.

The admittance matrix $\mathbf{Y}(z)$ obeys the generalized Riccati equation as follows from (1)

$$\partial_z \mathbf{Y} = -\mathbf{Y}\mathbf{T}_{eb}\mathbf{Y} + \mathbf{T}_{be}. \tag{4}$$

Boundary conditions for the admittance matrix are as follows: $\mathbf{Y} = \mathbf{Y}_g$ at $z = 0$ and $\mathbf{Y} = \mathbf{Y}_\infty$ at $z \to \infty$. The matrix $\mathbf{Y}_\infty$ is found by selection of a decaying solution of the dispersion equation in the topside ionosphere.
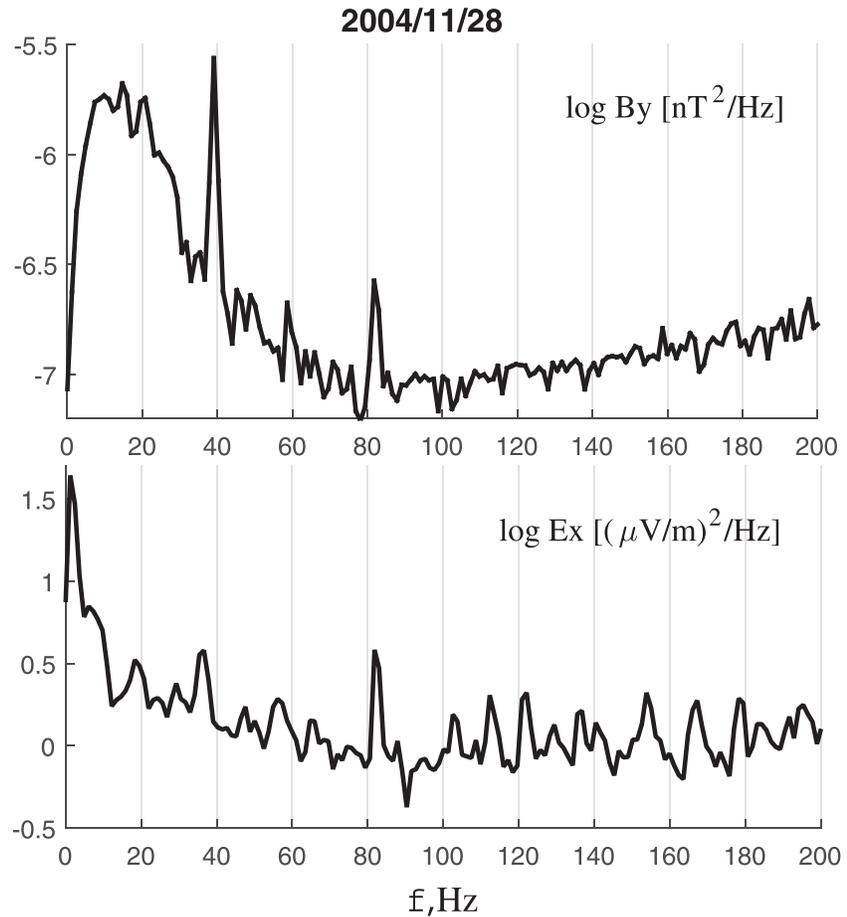
Figure 9. Power spectra of E_x and B_y components for the event of 28 November 2004 during time interval 09.10.00–09.10.20 UT.

Numerically solving the first Cauchi problem, we get the admittance matrix at altitudes below the source: $\mathbf{Y}(z) = \mathbf{Y}^-(z)$ at $z < h$, whereas the numerical solution of the second Cauchi problem gives us the admittance matrix above it: $\mathbf{Y}(z) = \mathbf{Y}^+(z)$ at $z > h$. At the source level $z = h$ the admittance matrix has the characteristic discontinuity. From that, the horizontal components of the electric and magnetic field can be found

$$\mathbf{e}_\tau(h) = \left[\mathbf{Y}^+(h+0) - \mathbf{Y}^-(h-0)\right]^{-1}\mathbf{s}, \mathbf{b}_\tau(h\pm0) = \mathbf{Y}^\pm(h\pm0)\mathbf{e}_\tau(h). \tag{5}$$

Then, starting from these values as the boundary conditions at $z = h \pm 0$, one may numerically solve two Cauchi problems for Maxwell's equation (1) upward and downward from the source level. This way the horizontal components of the electromagnetic field $\mathbf{e}_\tau(z)$ and $\mathbf{b}_\tau(z)$ can be found at any altitude.

The stability of the numerical solution of Maxwell's equations is significantly improved by step-by-step corrections using the precomputed admittance matrix $\mathbf{Y}(z)$. Upon the cyclotron resonance at some altitude, the coefficients of Maxwell's equations experience rapid variations, which may result in the numerical instability of the Runge-Kutta method. However, at the considered frequency no cyclotron resonance condition is met within the ionosphere.

4. Modeling the Electromagnetic Emission Produced by the ZEVS Transmitter

The IRI parameters have been chosen to correspond to winter nighttime conditions (LT = 21) during 8 December 2007 event and latitude 69° corresponding to the ZEVS location. The IRI-derived static Pedersen and Hall conductances are $\Sigma_P = 0.04$ S and $\Sigma_H = 0.12$ S; the peak height is $h_mF2 = 303$ km, and the total ionospheric content (integration from 50 to 2,000 km) is TEC = 0.5 TECu. The ZEVS installation is located at a crystalline shield with a very high resistance $\sim 10^5$ Ohm·m (the corresponding skin depth at 82 Hz is
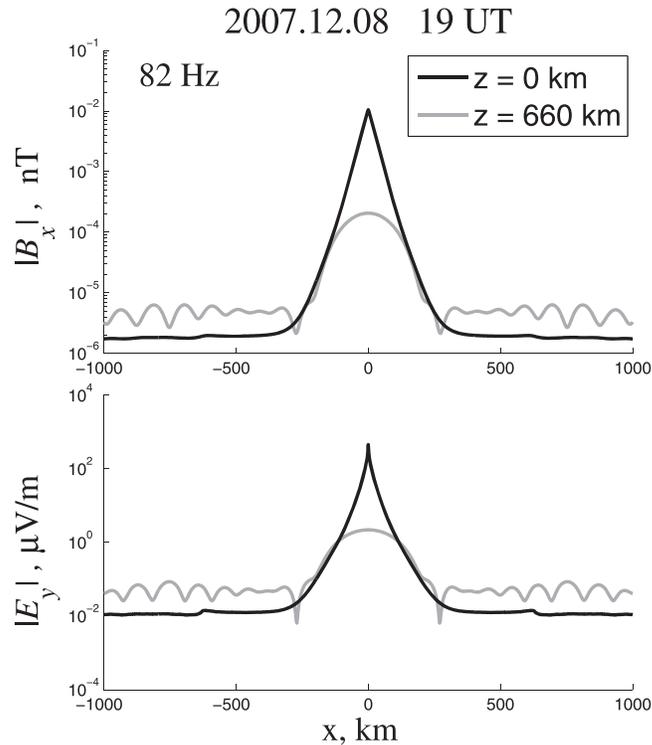
Figure 10. The spatial structure of magnitudes of the magnetic component $|B_x(z)|$ (upper panel) and electric component $|E_y(x)|$ (bottom panel) of electromagnetic emission generated by an infinite line current oscillator at $f = 82$ Hz on the ground (black line) and in the upper nighttime ionosphere (gray line).

$\delta_g \simeq 16$ km). The atmospheric conductivity is taken to be $\sigma_a = 1.1 \cdot 10^{-14}$ S/m at the ground surface and increases exponentially to the altitude of 80 km to match the IRI-deduced conductivity. According to the IGRF model, the magnetic field inclination at the ZEVS location is $I = 78°$. Because the distinction from the vertical magnetic field is small, we assume that $I = 90°$.

As a first step, we allow that the line source current is infinitely long. This assumption will somewhat overestimate the effect from a realistic current with a finite length $L = 60$ km. The calculated field components correspond to the source current $J_0 = 1$ A.

4.1. ELF Signal Propagation Away From the Transmitter

The propagation of ELF signals generated by a power transmission line along the Earth's surface was well described theoretically and verified experimentally. Here we provide the results of our modeling to validate the model's consistency with known observational results. Figure 10 shows the spatial structure across the line current of the electromagnetic field excited by current oscillations at 82 Hz on the ground ($z = 0$) and in the upper ionosphere ($z = 660$ km). On the ground, up to the distances ~300 km, the amplitude of electromagnetic disturbance decays nearly exponentially $\propto \exp(-x/L_x^{(g)})$ with scale $L_x^{(g)} \simeq 33$ km. At larger distances, >300 km, the decay rate becomes very low; for the distances between 400 and 900 km the estimate of decay scale is $L_x^{(g)} \simeq 3,000$ km. In the upper ionosphere, the field decrease rate for the electric and magnetic components is nearly the same as on the ground, $L_x^{(i)} \simeq 30$ km (for the distances 50–300 km).

To verify the validity of our model, we compare the model predictions with previous observational results at two distant stations (see map in Figure 1; Sidorenko et al., 2014). At the Petrozavodsk site (distance from ZEVS installation $R \simeq 780$ km) the 82-Hz signal was recorded with amplitude $B \simeq 2.1$ fT, whereas our model for $\sigma_g = 10^{-5}$ S/m gives $B \simeq 1.84$ fT (1 fT=10^{-15} T).The modeled result differs from observations only by a factor of ~ 0.9. At the Storozhno (STZ) site (distance from ZEVS $R \simeq 920$ km) the ZEVS signal was recorded with amplitude $B \simeq 1.5$ fT, whereas our model gives $B \simeq 1.7$ fT. The modeled result differs from observations by a factor of ~1.16 only. Thus, our modeling results closely coincide (within ~10%) with previous observational results.
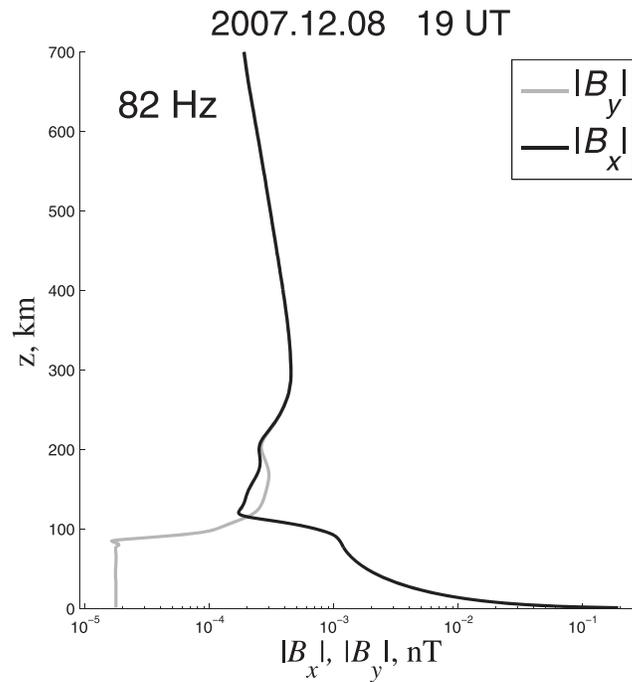
Figure 11. The altitudinal profile (nighttime conditions: 19 UT on 8 December 2007) of magnetic component magnitude $|B_x(z)|$ and $|B_y(z)|$ of electromagnetic emission generated by a ground line current oscillating at $f = 82$ Hz.

4.2. Vertical Structure of ELF Signals in the Ionosphere

The vertical structure of the amplitude of magnetic components is shown in Figure 11. In the upper ionosphere ($z \simeq 300$–700 km) the ELF transverse magnetic fieldd $|B_x|$ and $|B_y|$ generated by 1-A line current can reach up to ~1 pT. The parallel magnetic component $|B_z|$ vanishes above the line current.

The vertical structure of the amplitude of transverse electric components $|E_x|$ and $|E_y|$ is shown in Figure 12. Their amplitudes in the upper night side ionosphere produced by 1-A current may reach up to ~2 μV/m. Notice that the vertical profile of wave amplitudes is non-monotonic, in particular, the E field increases slowly above 300 km (Figure 12). Surely it does not mean that wave acquires energy upon upward propagation. These variations are the effect of wave propagation in an inhomogeneous medium. In a formal way, the wave amplitude behavior can be interpreted in the WKB approximation as follows: the equations for E and B differ by the term with first-order derivative ($\propto d\varepsilon/dz$). As a result, in the WKB solution for E field the pre-exponential factor is $\propto 1/\sqrt{n(z)}$ (where n is the refraction index), whereas for B field it is $\propto \sqrt{n(z)}$. Therefore, $E(z) \propto B(z)/n(z)$, and at altitudes $z > 300$ km the field $E(z)$ must increase with altitude, because $n(z) = k_z(z)/k_0$ decreases with altitude faster than $B(z)$ does.

4.3. Polarization Structure of ELF Emission in the Ionosphere

The absorption rate of the emission in the ionosphere $\propto \exp(-\text{Im}k_z)$ can be evaluated from asymptotics (2). Figure 13 (bottom panel) compares the local values of damping factors $\text{Im}k_z(z)$ for the emissions with LH polarization (with ion-like rotation) and RH polarization (with electron-like rotation). The exponential decrease with the height occurs with a characteristic scale $L_z \simeq 1/\text{Im}k_z$. This scale is $L_z < 10$ km for the LH mode and $L_z \simeq 100$–1,000 km for the RH mode in the bottom ionosphere; at $z > 200$ km the decay of RH mode becomes even more weak. Therefore, in the upper ionosphere only a mode with RH polarization can be observed.

The comparison of the local dissipation factor $\text{Im}k_z(z)$ for both modes for the day 8 December 2007 during daytime 07 UT (gray line) and nighttime 07 UT (black lines) is given in the bottom panel of Figure 13. This comparison evidences that wave dissipation during daytime is higher than during nighttime.

Figure 13 (middle panel) shows that the theoretically predicted emission ellipticity κ (signed ratio between small and large axes of the polarization ellipse). On the ground and in the atmosphere ($z < 100$ km) $\kappa \to 0$. This value corresponds to a linearly polarized disturbance on the ground produced by an infinite linear
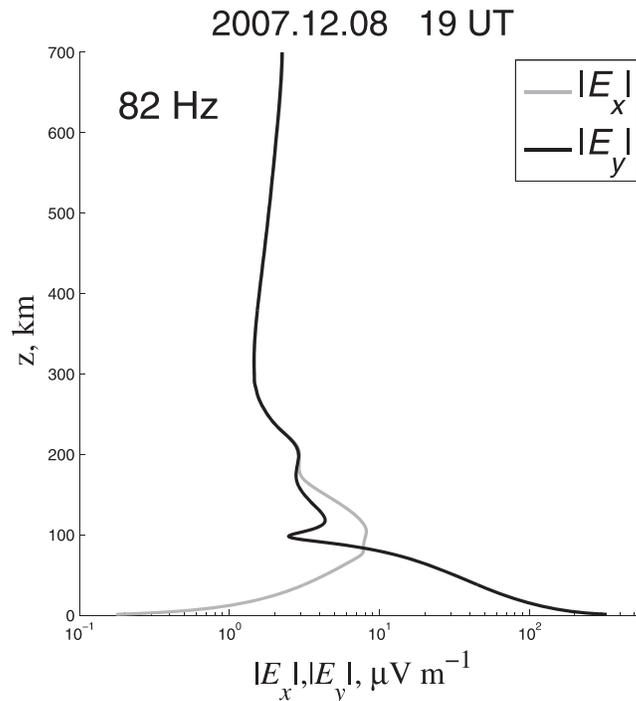
Figure 12. The altitudinal profile (the same nighttime conditions as in Figure 11) of electric component magnitude $|E_x(z)|$ and $|E_y(z)|$ of electromagnetic emission generated by a ground 82-Hz transmitter.

current. But in the ionosphere ($z > 150$ km) the ellipticity $\kappa \to 1$ which corresponds to RH circular-polarized wave. The modeling predictions fit perfectly the polarization properties of the emission recorded by the DEMETER magnetometer (Figure 7).

Figure 13 interprets the transformation of a linearly polarized signal generated by a ground extended transmitter into a circularly polarized wave in the upper ionosphere. Formally, a linearly polarized signal can be imagined as a combination of two oppositely polarized circular signals. In the ionosphere, a signal with one polarization is severely absorbed; therefore, in the upper ionosphere only a signal with other circular polarization is observed.

5. Discussion

The propagation of ELF signals generated by ZEVS transmitter along the Earth's surface has been successfully described theoretically and verified experimentally. The estimate of the horizontal decay of the ELF wave amplitude made with our model correspond well with the earlier modeling and observational results.

The developed theoretical model predicts that in the upper nightside ionosphere above a ground transmitter the electric component of ELF emission with amplitude ~400 μV/m may be expected from a linear oscillating 200-A current corresponding to typical ZEVS transmitter intensity. This modeling result corresponds to the most favorable conditions, when a satellite is exactly above the source. About 200(500) km away, the emission amplitude should be about 10(40) times less (Figure 10). Such disturbances with amplitudes about few tens of microvolts per meter have been indeed detected by electric sensor onboard DEMETER.

At the same time, the predicted amplitude of magnetic signal is to be ~ 40 pT above the transmitter ($R = 0$). About 200(500) km away, the emission amplitude should be about 2(1) pT. Such disturbances with amplitudes ~1–4 pT have been indeed detected by onboard magnetometer. Amplitudes of the ZEVS generated emissions renormalized to the location above a source ($R = 0$) detected during a daytime event (28 November 2004) were weaker as compared with those recorded during nighttime events (8 December 2007 and 6 March 2009). This observational fact indicates a larger absorption of ELF emission in the daytime ionosphere as compared with nighttime conditions.
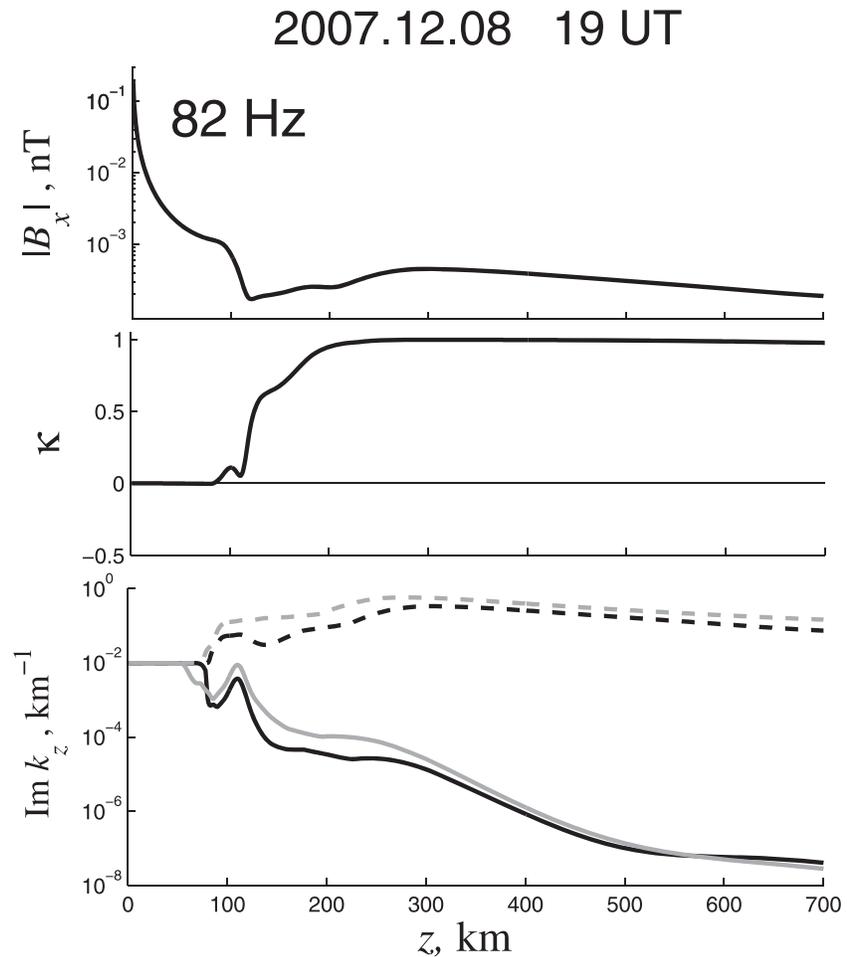
Figure 13. The altitudinal profile of the emission magnitude in $|B_x(z)|$ component (upper panel), ellipticity (signed ratio between small and large axes of the polarization ellipse) $\kappa(z)$ (middle panel), and imaginary part of the field-aligned wave vector $k_z(z)$ of RH-polarized mode (solid lines) and LH-polarized mode (dashed lines), generated by a ground line current oscillator at $f = 82$ Hz during nighttime 19 UT on 2007/12/08 (black lines). The gray lines correspond to daytime conditions (07 UT) on the same day.

The developed model has some simplifications. For simplicity the geomagnetic field has been assumed to be vertical. The account for a finite inclination of the geomagnetic field ($I = 78°$) will not modify the results considerably. However, the geomagnetic field can provide some guidance for electromagnetic emission, so as a result an equatorward shift of maximum response in the ionosphere to a ground ELF transmitter should be observed. Indeed, Figure 1 shows a tendency of the shift to lower latitudes of the regions with electromagnetic emission occurrence detected by DEMETER.

Though the assumption about an infinite line current is a reasonable approximation, it provides somewhat overestimated effects as compared with a finite length $L = 60$-km case. Further modeling efforts are needed to account for a finite scale of the line current L.

The observations presented here validated by the numerical modeling have proved that natural or man-made ELF electromagnetic activity near the ground can be monitored by LEO satellites (Simoes et al., 2012).

6. Conclusions

So far, the propagation of ELF signals generated by ground transmitters was modeled and experimentally validated only along the Earth's surface. We have numerically estimated the penetration into the realistic ionosphere of ELF emission from a ground source modeled as an infinite line current. The modeling shows that ELF signals from such a source with current intensity about 200 A can be reliably detected by electric

and magnetic sensors onboard the LEO satellite at horizontal distances up to ∼500 km. The modeling results are well supported by the DEMETER observations in the vicinity of the ZEVS ELF transmitter.

References

Berthelier, J. J., Godefroy, M., Leblanc, F., Malingre, M., Menvielle, M., Lagoutte, D., et al. (2006). ICE, the electric field experiment on DEMETER. *Planetary Space Science*, *54*, 456–471. https://doi.org/10.1016/j.pss.2005.10.016

Fedorov, E., Mazur, N., Pilipenko, V., & Baddeley, L. (2016). Modeling the high-latitude ground response to the excitation of the ionospheric MHD modes by atmospheric electric discharge. *Journal Geophysical Research: Space Physics*, *121*, 11,282–11,301. https://doi.org/10.1002/2016JA023354

Fraser-Smith, A. C., & Bannister, P. R. (1998). Reception of ELF signals at antipodal distances. *Radio Science*, *33*, 83–88.

Ginzburg, V. L. (1970). *The propagation of electromagnetic waves in plasmas*. Oxford: Pergamon Press.

Inan, U. S., Cummer, S. A., & Marshall, R. A. (2010). A survey of ELF and VLF research on lightning-ionosphere interactions and causative discharges. *Journal of Geophysical Research*, *115*, A00E36. https://doi.org/10.1029/2009JA014775

Interaction (2014). Interaction of electromagnetic fields of ELF controlled sources with the ionosphere and Earth's crust. In E. P. Velikhov, & Y. L. Voytekhovsky (Eds.), *Proceedings of the All-Russian Research and Practice Workshop (in 2 Volumes)*: Russ. Acad. Sci., Geological Institute Kola Science Centre. Apatity, 2014. 206 pp. ISBN 978-5-902643-23-4.

Lehtinen, N. G., & Inan, U. S. (2008). Radiation of ELF/VLF waves by harmonically varying currents into a stratified ionosphere with application to radiation by a modulated electrojet. *Journal of Geophysical Research*, *113*, A06301. https://doi.org/10.1029/2007JA012911

Mazur, N. G., Fedorov, E. N., Pilipenko, V. A., & Vakhnina, V. V. (2018). ULF electromagnetic field in the upper ionosphere excited by lightning. *Journal of Geophysical Research: Space Physics*, *123*, 6692–6702. https://doi.org/10.1029/2018JA025622

Means, J. D. (1972). Use of the three-dimensional covariance matrix in analyzing the polarization properties of plane waves. *Journal of Geophysical Research*, *77*, 5551–5559.

Nickolaenko, A. P. (2008). ELF attenuation factor derived from distance dependence of radio wave amplitude propagating from an artificial source. *Telecommunications and Radio Engineering*, *67*(18), 1621–1629.

Nickolaenko, A. P., Shvets, A. V., & Hayakawa, M. (2016). Extremely low frequency (ELF) radio wave propagation: A review. *International Journal of Electronics and Applied Research*, *3*(2), 81. (http://eses.co.in).

Parrot, M., et al. (2006). The magnetic field experiment IMSC and its data processing onboard DEMETER: Scientific objectives, description and first results. *Planetary Space Science*, *54*, 441–455.

Parrot, M. (2018). DEMETER observations of manmade waves that propagate in the ionosphere. *Comptes Rendus Physique*, *19*, 26–35. https://doi.org/10.1016/j.crhy.2018.02.001

Rothkaehl, H., & Parrot, M. (2005). Electromagnetic emissions detected in the topside ionosphere related to the human activity. *Journal of Atmospheric Solar-Terrestrial Physics*, *67*, 821–828.

Santolik, O., Lefeuvre, F., Parrot, M., & Rauch, J. L. (2001). Complete wave-vector directions of electromagnetic emissions: Application to INTERBALL-2 measurements in the night-side auroral zone. *Journal Geophysical Research*, *106*, 13,191–13,201.

Santolik, O., Parrot, M., & Lefeuvre, F. (2003). Singular value decomposition methods for wave propagation analysis. *Radio Science*, *38*(1), 1010. https://doi.org/10.1029/2000RS002523

Sidorenko, A. E., Tereshchenko, E. D., Tereshchenko, P. E., & Grigoriev, V. F. (2014). Features of ELF electromagnetic waves propagation along subauroral path. In *"Radiowave propagation": XXIV all-Russian conference, Irkutsk, V.2.*, pp. 259–262.

Simoes, F., Pfaff, R., Berthelier, J.-J., & Klenzing, J. (2012). A review of low frequency electromagnetic wave phenomena related to tropospheric-ionospheric coupling mechanisms. *Space Science Review*, *168*, 551–593.

Starks, M. J., Quinn, R. A., Ginet, G. P., Albert, J. M., Sales, G. S., Reinisch, B. W., & Song, P. (2008). Illumination of the plasmasphere by terrestrial very low frequency transmitters: Model validation. *Journal Geophysical Research*, *113*, A09320. https://doi.org/10.1029/2008JA013112

Tereshenko, E. D., & Tereshenko, P. E. (2017). Electric field of horizontal linear water-grounded aerial. *Journal of Technical Physics*, *87*, 453–457.

Wait, J. R. (1972). Project Sanguine. *Science*, *178*(4058), 272–5. https://doi.org/10.1126/science.178.4058.272

Wait, J. R. (1977). Propagation of ELF electromagnetic waves and project Sanguine / Seafarer. *IEEE Journal of Oceanic Engineering*, *2*, 161–172. https://doi.org/10.1109/JOE.1977.1145337

Yano, M., Ida, Y., Hobara, Y., Hayakawa, M., & Nickolaenko, A. P. (2010). Reception of ELF transmitter signals at Moshiri, Japan, and their propagation characteristics. *Radio Science*, *45*, RS1009. https://doi.org/10.1029/2009RS004224

Zhamaletdinov, A. A., Shevtsov, A. N., Velikhov, E. P., et al. (2015). Study of interaction of ELF-ULF range (0.1-200 Hz) electromagnetic waves with the Earth's crust and the ionosphere in the field of industrial power transmission lines (FENICS experiment). *Izvestiya - Atmospheric and Oceanic Physics*, *51*, 826–857.